RSC Advances

PAPER

View Article Online
View Journal | View Issue

Cite this: *RSC Adv.*, 2022, **12**, 24311

Exploring the evolution patterns of melem from thermal synthesis of melamine to graphitic carbon nitride†

Yuhui Yi, ‡ Jie Wang, ‡ Yingli Niu, Yu Yu, Songmei Wu * and Kejian Ding *

Received 28th May 2022
Accepted 21st July 2022

DOI: 10.1039/d2ra03337b

rsc.li/rsc-advances

In the exploration of synthesizing graphitic carbon nitride (g-C_3N_4), the existence of secondary anime bridging units shows the incompleteness of related theories. Thus, taking the thermal synthesis of melamine as an example, this work finds a possible reaction path with Density Functional Theory (DFT) for forming melem during the thermal synthesis of g-C_3N_4. Combined with transition state theory (TST), it indicates that the formation of melem results from the condensation of melamine and isomerization of melam. Meanwhile, the weak signal near 2135 cm^{-1} in the Fourier Transform Infrared Spectra (FTIR) corresponds to the vibration of carbodi-imines (–N=C=N–), which further proves the proposed reaction path. Thus, this work can explain the formation of g-C_3N_4 and its monomer, which may contribute to the successful formation of ideal g-C_3N_4 in the future.

1 Introduction

Graphitic carbon nitride (g-C_3N_4) is a quasi-planar material with low density, high chemical stability, and good biological compatibility, and has broad applications in membrane materials,[1] catalysts and catalyst supports,[2] and the preparation of metal nitrides.[3] As shown in Fig. 1, there are three possible structures of g-C_3N_4, which are triazine-based g-C_3N_4 (TGCN), heptazine-based g-C_3N_4 (HGCN), and melon-based g-C_3N_4 (MGCN), and two derivatives including poly (triazine imide) (PTI) and poly (heptazine imide) (PHI). In 1996, Teter and Hemley proposed five possible carbon nitride structures, namely, α-phase, β-phase, cubic phase, pseudo cubic phase, and graphitic phase.[4] Although there was a lack of concrete evidence and precise characterization, g-C_3N_4 was described as TGCN (Fig. 1(a)) in their work and related research.[5–7] However, based on the paper of Kroke *et al.* in 2002, HGCN (Fig. 1(b)) is thermodynamically preferential to TGCN and widely used as a schematic of g-C_3N_4 in many papers.[8] Moreover, the use of nuclear magnetic resonance (NMR) and Fourier-transform infrared spectroscopy (FTIR) was successful to distinguish triazine and heptazine, which made these two methods regarded as essential characterization methods for the study of g-C_3N_4 and relevant compounds. Nevertheless, both TGCN and HGCN are ideal 2D structures, and the lack of (110) signal in X-ray powder diffraction (XRD) raised doubts if 2D structures existed in the product until 2007 when Lotsch *et al.* showed the existence of MGCN (Fig. 1(c)).[9] Specifically, almost all g-C_3N_4 synthesized by experiments is composed of melon, which is a 1D polymer and connects each other by hydrogen bonds and weak interactions. Additionally, Fina *et al.* further demonstrated this structure with XRD and neutron diffraction in 2015.[10] It indicated that MGCN is the most accurate structure of g-C_3N_4 obtained by experiments. Notwithstanding g-C_3N_4 with an ideal 2D structure was not gotten as expected, researchers found the existence of PTI (Fig. 1(d)) and PHI (Fig. 1(e)). In 2008, Thomas *et al.* claimed that HGCN was obtained by ionothermal synthesis with KCl and LiCl,[11] which method could overcome the diffusion limitation of reactant (such as melamine) and intermediates (including melam and melem), but the following characterization such as nuclear magnetic resonance (NMR) crystallography proved that the 2D network belonged to PTI.[12] Moreover, Lotsch *et al.* synthesized PHI successfully in 2019 including K–PHI and H–PHI,[13] while it was structurally determined in 2009 by Döblinger's group.[14] In this case, it is an interesting question why there seem no tertiary but secondary amines bridge units in actual products including MGCN, PTI, and PHI.

As mentioned before, there are three key molecules to analyse the mechanism of g-C_3N_4 formation, which are melamine, melam, and melem. Specifically, melamine (2,4,6-triamino-*s*-triazine), $C_3N_3(NH_2)_3$, is a precursor for the synthesis of g-C_3N_4, which can form a dimer named melam. Besides, melamine is easy to sublime, and its melting point is 345 °C. Meanwhile, melem (2,5,8-triamino-tri-*s*-triazine), $C_6N_7(NH_2)_3$, is regarded as a monomer of HGCN, MGCN, and PHI, which may be generated from melamine and/or melam. In 2003, Schnick *et al.* reported the synthesis and structural analysis of melem,

School of Science, Beijing Jiaotong University, Beijing 100044, P.R. China. E-mail: dkjian@bjtu.edu.cn; smwu@bjtu.ed.cn

† Electronic supplementary information (ESI) available. See https://doi.org/10.1039/d2ra03337b

‡ These authors contributed equally to this work.

and they indicated that the formation of melem might relate to the decomposition from melamine to cyanamide or dicyandiamide (Fig. S1†).[15] Moreover, based on the X-ray analysis and differential scanning calorimetry (DSC), Antonietti *et al.* showed that the formation of cyameluric core occurs near 390 °C.[16] Besides, the temperature used to synthesize graphitic carbon nitride is generally set as 550 °C. However, it is strange that the mechanism of reaction from melam to melem has not been illustrated yet. Considering the stability of melamine, there still is a question if the decomposition dominates the reaction, which means it is worth pondering the competitive relationship between the decomposition and the condensation polymerization.

Thus, the existence of secondary amines that bridge units and the conversion from triazine units to heptazine units deserve further research. Taking the development history of carbon nitride into account, theories and simulations were essential to indicate the directions of the research, while experiments and characterizations demonstrated whether these directions were correct or not. People prefer to obtain an ideal g-C_3N_4 whether TGCN or HGCN, but the product composed of MGCN or just melon means that the related theories should be further improved. For example, Botari *et al.* showed the thermodynamic equilibrium among melem, melon, and MGCN by density functional theory (DFT).[17] It indicated the broad stability area of melon for common thermal synthesis, but the specific reaction path was not taken into consideration. Therefore, it is necessary to reveal possible intermediates and the complete polymerization process through simulations, which may solve the difficulty to monitor the reaction path by experiment. As one of the popular and useful methods in the fields of computational physics and computational chemistry, DFT is an important tool to explore the properties of materials, including corresponding structures, possible spectra, and chemical reaction mechanisms. Thus, it will be useful to figure out the possible reaction path from melamine to melem with DFT. Generally, the results of geometry optimizations and frequency calculations obtained by B3LYP method are reasonable for systems of main-group elements and ordinary organics.[18–20] Considering the dispersion correction, it is feasible to find intermediates and transition states (TS) by B3LYP-D3(BJ) method, which may help to describe the formation of melem from the thermal synthesis of melamine to g-C_3N_4.[21,22] Moreover, the thermodynamic data obtained from the DFT calculation will help to analyse the ideal reaction rate and reaction time by transition-state theory (TST).

Accordingly, this article will explain the formation of melem from melamine to g-C_3N_4 by finding possible intermediates and transition states with DFT, during which people can understand the role of secondary amine for bridging units and the process of isomerization of melam. Moreover, this work may help to save time and cost when researchers try to synthesize ideal g-C_3N_4 in the future.

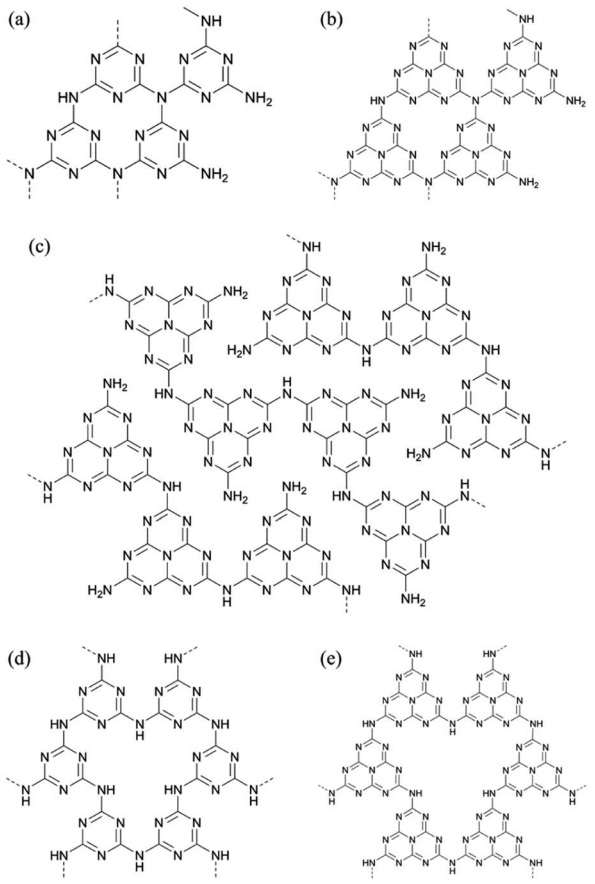

Fig. 1 Graphitic carbon nitride (g-C_3N_4) and its derivatives: (a) triazine-based g-C_3N_4 (TGCN), (b) heptazine-based g-C_3N_4 (HGCN), (c) melon-based g-C_3N_4 (MGCN), (d) poly (triazine imide) (PTI) and (e) poly (heptazine imide) (PHI).

2 Materials and methods

2.1 Materials

Melamine (99%) was bought from Innochem. The High Temperature Furnace (OTF-1200X-II) was used to heat reactants. Meanwhile, the samples were heated to 360 °C at the heating rate of 10 °C min^{-1} in a nitrogen atmosphere, and the samples were preserved for 5, 10, 20, 40, 60, 120, 240, 360, 480, and 600 minutes followed by natural cooling. The Fourier Transform infrared spectroscopy (FTIR) was carried out on the IRTracer-100, SHIMSDZU.

2.2 Methods

The DFT calculation is based on Gaussian 16, and B3LYP/6-31g(d) is used for optimization and frequency calculation with DFT-D3(BJ) correlation, in which the correction factor is 0.9614.[23–25] Meanwhile, revDSD-PBEP86-D3(BJ)/cc-pVTZ is applied to get corresponding energy of the single point with higher accuracy.[26] Furthermore, Shermo is a useful code for calculating thermodynamic data based on ideal gas assumptions, and Shermo 2.1 was used to refine the thermodynamic data obtained by B3LYP/6-31g(d) with single point energy gotten by revDSD-PBEP86-D3(BJ)/cc-pVTZ, which can reduce calculation time and ensure the precision and accuracy of the results.[27] Moreover, the Gibb free energy corresponds to the sum of

electronic energy and thermal correction. The visualization of 3D structures is made by CYLview20.[28] Besides, conformation search for flexible intermediates was procced by dynamics simulation *via* molclus 1.9.9.5 combined with xtb.[29–32] Additionally, Interaction Region Indicator (IRI) analysis was used to reveal weak interactions and chemical bonds by Multiwfn 3.7 and presented by Visual Molecular Dynamics (VMD).[23,33,34] Lastly, the concentration of substances as a function of reaction time or temperature was calculated by Python.[35]

3 Results and discussion

3.1 Unimolecular reactions of melamine

As indicated previously, the formation of melem may relate to the decomposition of melamine to cyanamide or dicyanamide, and it is necessary to know the corresponding energy during the reaction, such as Gibbs free energy (G). Because of the structural difference, dicyandiamide is considered as the synthesized product of two cyanamides rather than the direct product of melamine, which means the transition state from melamine to cyanamides deserves to be concerned about. As shown in Fig. S2,† the change of Gibbs free energy (ΔG) for the transition state is +103.9 kcal mol^{-1} during the decomposition process. Generally, for unimolecular reactions including isomerization and decomposition, the energy barrier for spontaneous reactions at room temperature is lower than +21 kcal mol^{-1}. Furthermore, when the barrier is +76.5 kcal mol^{-1}, the half-life of the unimolecular reaction is as high as 12.8 hours at 650 °C.[36] Thus, it can be assumed that melamine is stable enough.

Although the decomposition of melamine is difficult to happen which involves three broken bonds, the energy provided by the surrounds will ensure the existence of the tautomeric forms of melamine and melam,[15,37,38] and hydrogen atoms can move from amino to triazine. It is worth noting that the migration of hydrogen atom among nitrogen atoms can be regarded as sigmatropic rearrangements, and the process is similar to [1,3]-sigmatropic (σ[1,3]) migrations of hydrogen where the migration origin and terminus both are nitrogen atoms rather than carbon atoms.[39] Therefore, it is proposed that the tautomeric forms of melamine may result in just one broken bond, which process is connected to the isomerization of melamine as shown in Fig. 2. The intermediate states are on both sides of the black arrows, which have the local minimum energies. Meanwhile, the transition states are above the black arrows, which have the local maximum energies. Moreover, the green arrows mean the vibration directions and the bonds in red are concerned about during the isomerization process.

Combined with Fig. S3,† the reaction from M1 to M3 corresponds to the σ[1,3] migration of hydrogen atom between nitrogen atoms, and M3 is a kind of tautomeric forms of melamine as mentioned in the references. Then, the remained solitary hydrogen of M3 may vibrate to the other side. Thus, the ring can open as illustrated from M5 to M7 with the formation of carbodi-imine (–N=C=N–H). Although the nucleophilic of carbodi-imine (–N5=C6=N7–H8) and the electrophilic of imine (=N10–H9) make molecule M7 easy to form triazine again, the structure's flexibility may ensure the existence of this structure. In short, the isomerization of melamine is composed of the migration and vibration of hydrogen atoms and the formation of carbodi-imine.

As for the method to obtain thermodynamic data, the inconsistency of the potential energy surfaces with B3LYP-D3(BJ) and revDSD-PBEP86-D3(BJ) may result in a significant error, but Shermo can deal with this relatively systematic error well, which is shown in Fig. 3 and S4.† As stated by Grimme *et al.*, B3LYP-D3(BJ) may provide reasonable data in the field of molecular thermochemistry,[40] but the results processed with Shermo are closer to the thermodynamic data gotten by revDSD-PBEP86-D3(BJ) directly. Thus, it is feasible to use Shermo to get thermodynamic data during the reaction, and the energy barriers are lower than 50 kcal mol^{-1}. Moreover, it is worth noting that the proportion of melamine dominates the mixture because of its lowest Gibbs free energy and stable stability, but the process of isomerization of melamine may influence the formation of melem from melam or melamine chain.

3.2 Condensation of melamine or melem

The discussion of decomposition and isomerization of melamine is caused by the competition between the formation of the melamine chain and transformation from melamine to melem. If two melamine molecules are close to each other, there will be two situations due to the steric effects. On the one hand, when the nitrogen atom of the amino group is connected to another hydrogen atom of the adjacent melamine, the condensation reaction is almost impossible because of the hydrogen bond. On the other hand, if the nitrogen atom of the amino group relates to the carbon atom rather than the hydrogen atom, there seems

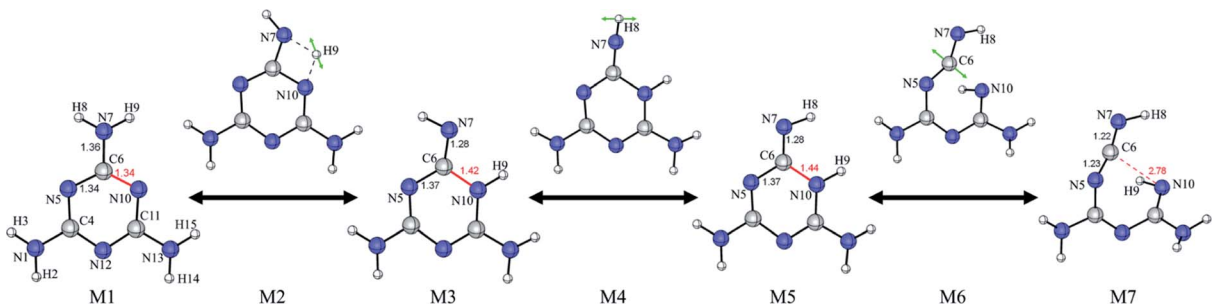

Fig. 2 The isomerization process of melamine. M1: melamine; M3, M5, M7: intermediates; M2, M4, M6: transition states.

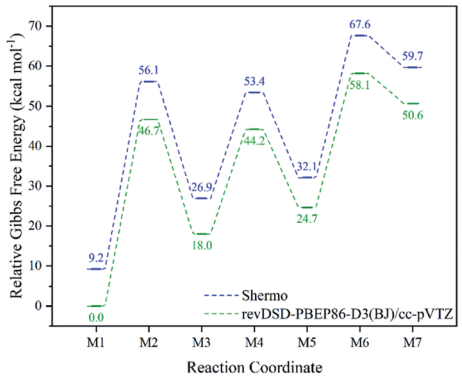

Fig. 3 The relative Gibbs free energies for melamine's isomerization.

no possible hydrogen atom left for the deamination. Thus, the tautomeric form of melamine (M3 in Fig. 2) is taken into consideration, where the hydrogen atom on the ring ensures that the deamination occurs, and the strong nucleophilicity and high degree of freedom of the nitrogen atom with a single hydrogen atom can be connected to the carbon atom of another ring.

Compared to $\Delta G = +103.9$ kcal mol^{-1} for the decomposition of melamine, ΔG for the condensation of melamine is +45.3 kcal mol^{-1} as shown in Fig. 4(a), where separated reactants/products correspond to isolated reactant/product molecules, and reactants/products mean reactant/product molecules with intermolecular interactions. Considering the formation of melamine's tautomeric form with $\Delta G =$ +46.9 kcal mol^{-1}, it can be proposed that the formation of melam or melamine chain has a higher possibility than the decomposition of melamine, which implies the rationality of isomerization of melamine, melam, and melamine chain. Furthermore, Fig. 4(b) presents the condensation of melem and its tautomeric form in a similar process.

The qualitative description may just provide an ambiguous result, but the thermodynamic data mentioned before can offer a quantitative display. Based on transition-state theory (TST), the concentration changes of melam after 30 minutes of reaction at different temperatures are shown in Fig. 5. It implies that the condensation process may need a reaction temperature higher than 390 °C to be detected. Moreover, as indicated in Table S1 and Fig. S5,† this process tends to complete near 30 minutes at 550 °C compared with the decomposition process, which proves that condensation of melamine dominates the reaction rather than decomposition. Although molecules are regarded as ideal gas molecules in the simulation, the high temperature and nitrogen atmosphere ensure the consistency between experiment and simulation. Furthermore, the steric effect can explain the reason why there seems no tertiary but secondary amine bridging triazine or heptazine units in MGCN, PHI, and PTI.

3.3 Formation of melem

Taking the condensation and isomerization or melamine into account, the formation of melem from melam might be described as follows. Firstly, the condensation polymerization of melamine occurs. During the period, the decomposition of melamine can happen but will not dominate the formation of melem. For the isomerization of melam, Fig. 6 presents the outline of the process, while all steps in the simulation are shown in Fig. S6† and the IRI analysis for the reaction is shown in Fig. S7.† Moreover, the conformation search for flexible molecules (T01, T03, T06, and T08) is stated in ESI,† and the specific Gibbs free energy variation is shown in Fig. S8.†

After the condensation, σ[1,3] migration and vibration of hydrogen atoms occur to open the triazine ring with the formation of carbodi-imines and imines. As shown from T01 to T02, after the first formation of carbodi-imine (–N5=C6=N7–H8) and imine (=N10–H9), the rotation will ensure the existence of different conformations including T02. Then, following the second formation of carbodi-imine (–N16=C17=N18–H19) and imine (=N21–H20), rotation and rearrangement can happen to form a new triazine, as illustrated from T02 to T06. Specifically, the formation of carbodi-imines is related to the accumulation of energy, and the rotations stabilize the

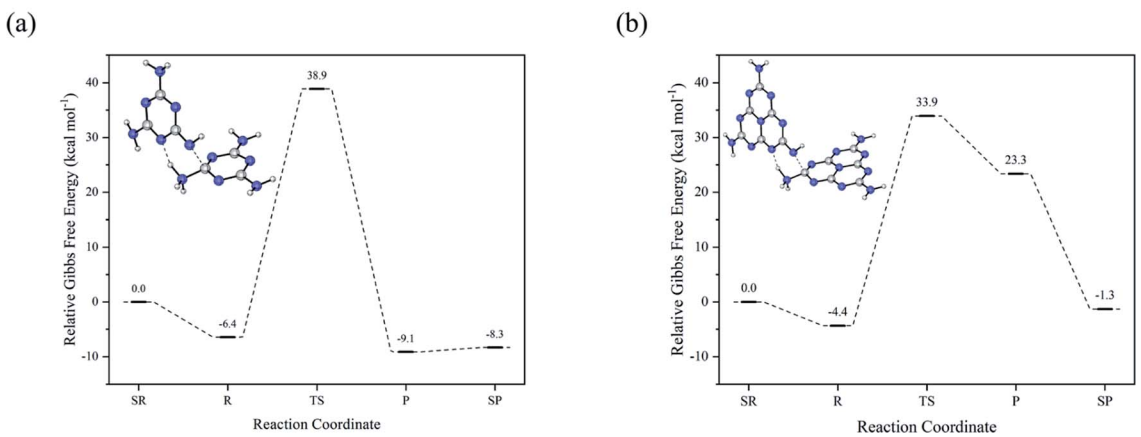

Fig. 4 The relative Gibbs free energies for the condensation of (a) melamine and (b) melem with their tautomeric forms. SR: separated reactants; R: reactants; TS: the transition state; P: products; SP: separated products.

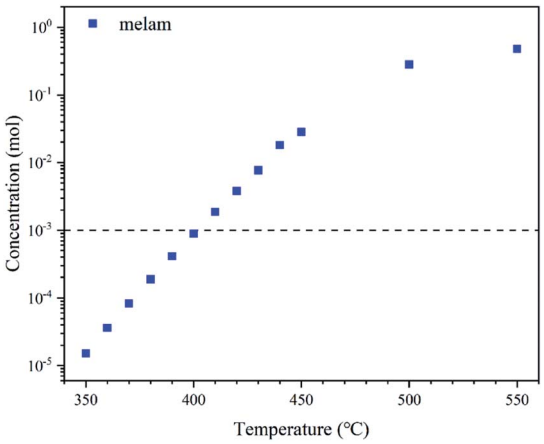

Fig. 5 The concentration of melam after 30 minutes of reaction at different reaction temperatures.

structures with a high degree of flexibility till the second carbodi-imine (–N16═C17═N18–H19) connects to the adjacent imine (═N10–H9). Meanwhile, as shown from T06 to T08, σ [1,3] migration of the hydrogen in the new ring will proceed, which will further stabilize the triazine. However, the high electrophilicity of the remained carbodi-imine (–N5═C6═N7–H8) makes this segment easily attracted by the N13 in the triazine to form the skeleton of heptazine, as shown from T08 to T09. For the formation of heptazine shown from T09 to T10, it is caused by the nucleophilicity of imine (═N7–H8) and the bonding of N7–C22. After that, deamination will occur to form the melem's tautomeric form, and the melem is obtained after its isomerization (Fig. S9–S11†). However, because the reaction occurs in an open system, it is difficult to detect and monitor this process, which also shows the importance of simulation. Then, TST can be used to further analyse the isomerization reaction.

The energy barriers for every step during the isomerization process are lower than 50 kcal mol^{-1}, and the reaction rate can be estimated based on these data. Ideally, rotations after formation of carbodi-imines will obstruct the reverse reactions, which makes the formation of carbodi-imines be regarded as irreversible steps. Meanwhile, after the formation of new triazine, σ[1,3] migration of hydrogen and rotations ensure the

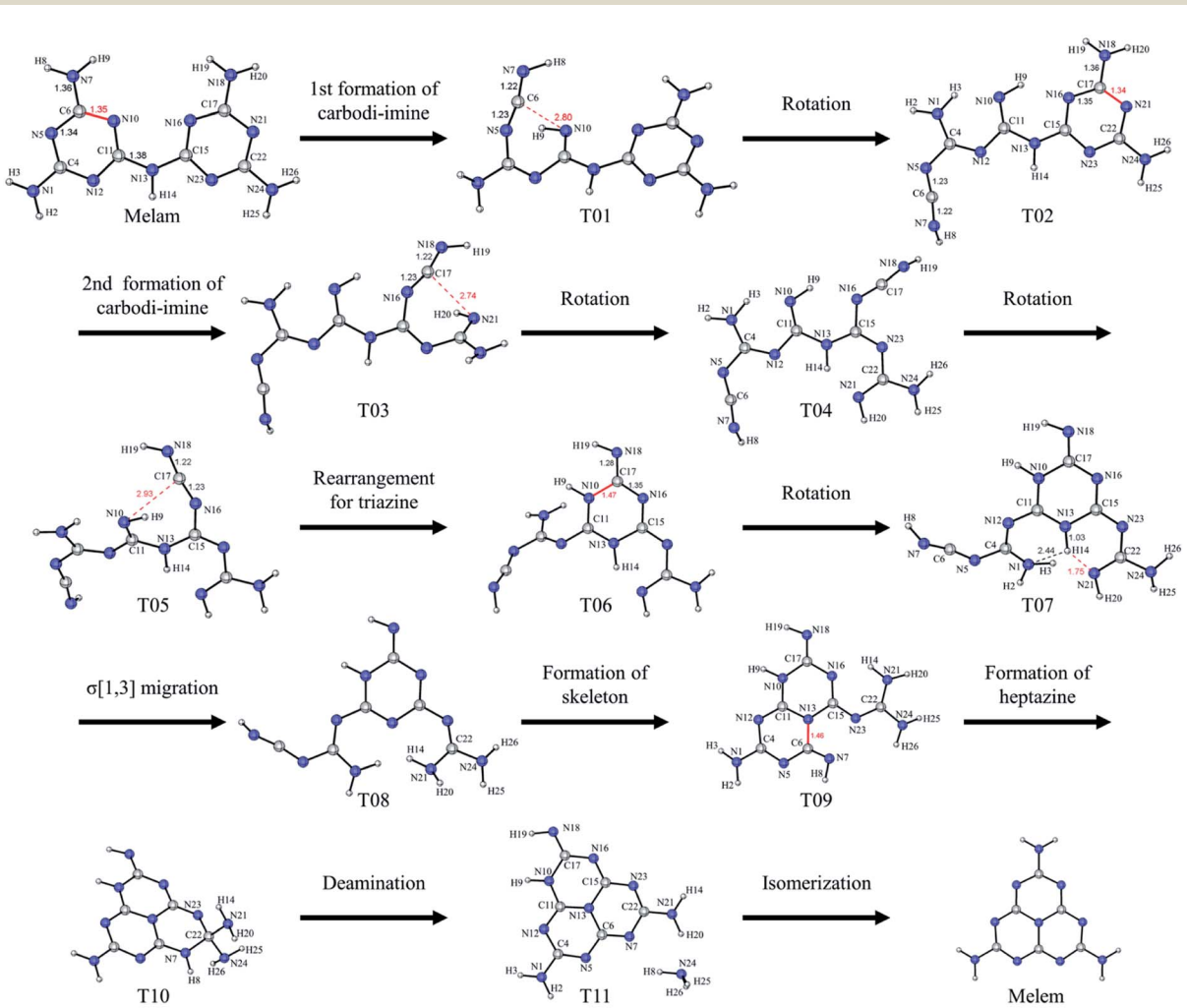

Fig. 6 Formation of melem from melam and its tautomeric forms (T01–T11).

Table 1 Equivalent reaction rates and reaction time for the isomerization of melam

Temperature (°C)	k_{iso} (s^{-1})	Half-life (Hours)	97% complete (Hours)
550	1.20×10^{-2}	0.02	0.08
500	1.18×10^{-3}	0.16	0.82
450	8.47×10^{-5}	2.27	11.50
400	4.12×10^{-6}	46.69	236.20
390	2.13×10^{-6}	90.19	456.27
360	2.62×10^{-7}	735.49	3720.75

decrease of relative Gibbs free energy of the molecule, and this continuous process is regarded as one step. Based on these assumptions, the reaction can be simplified with the corresponding reaction rates for each step shown in Table S2,† and the equivalent reaction rates (k_{iso}) and reaction time for the process are shown in Table 1. It shows the dependence of the reaction on temperature and proves the rationality of the isomerization of melam. Considering the condensation of melamine at the temperature higher than 390 °C, it also indicates that the temperature for the formation and condensation of melem should higher than 500

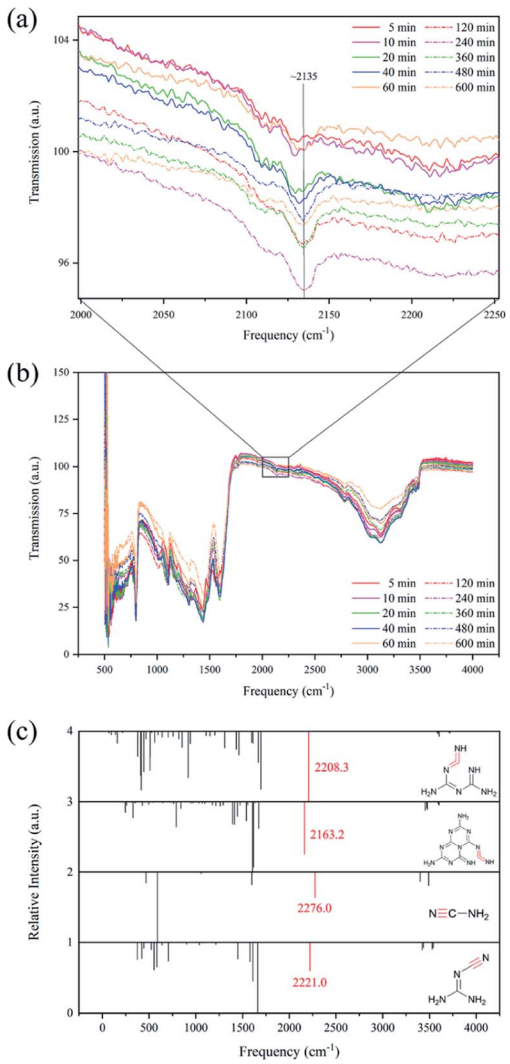

Fig. 7 The FTIR spectra of mixed products with frequencies in the region (a) 2000–2250 cm^{-1} and (b) 500–4500 cm^{-1}, and (c) IR simulation results of carbodi-imines in melamine's and melem's tautomers respectively and nitriles in cyanamide and dicyandiamide respectively (from top to bottom).

3.4 The FTIR results

The research of this reaction path began with the notice of FTIR signal in the region 2100–2300 cm^{-1}. Compared with the reaction paths proposed in the past, there is a vibration difference between carbodi-imine (–N=C=N–) and nitrile (–C≡N). The carbodi-imine is related to this scenario and the nitrile is relevant to the participation of dicyandiamide in the formation of melem, while it seems impossible to clear if cyanamide acts as the role of reactant. Conventionally, the vibration of nitrile (–C≡N) corresponds to the signal in the region 2200–2260 cm^{-1}, and cyanamides have an absorption in the region 2200–2225 cm^{-1}. Besides, aliphatic carbodi-imines (R–N=C=N–R) have an absorption in the region 2130–2155 cm^{-1}.[41] As shown in Fig. 7(a) and (b), the signal near 2135 cm^{-1} indicates the existence of carbodi-imines (–N=C=N–), which further proves the rationality of proposed isomerization process. Meanwhile, the variation of the intensity may show the reduction of nitrile left in the melamine industrial production process and increasing of carbodi-imine, as shown in Fig. S12.† Although the reaction took place in the molten and/or gas phases, FTIR was carried out in the solid state, which led to the difference between experimental results and simulation results. However, as shown in Fig. 7(c), the simulation results compare the vibration signals of carbodi-imines in melamine's and melem's tautomers with those of nitrile in cyanamide and dicyanamide, which agrees with the literature. Thus, the formation of melem from melamine results from condensation and isomerization.

4 Conclusions

In conclusion, this work shows a reaction path for the formation of melem from melamine, which can explain some problems during the experiment for the synthesis of g-C_3N_4. Firstly, the condensation polymerization of melamine or melem involves the participation of corresponding tautomeric forms, which can explain the existence of secondary anime bridging triazine or heptazine units in MGCN, PHI, and PTI. Then, σ[1,3] migration, vibration, and rotation dominate the isomerization process, which is proved by DFT and TST results. Meanwhile, TST results indicate that the condensation of melamine may be detected above 390 °C, while the isomerization and condensation of melem require a temperature higher than 500 . Lastly, the FTIR signal near 2135 cm^{-1} refers to the vibration of carbodi-imines rather than nitriles, which further proves the rationality of the proposed isomerization process. Therefore, this work provided a more appropriate reaction path to describe the formation of melem, which may contribute to the successful

synthesis of g-C_3N_4 with perfect network structure in the future if the steric effects can be dealt with.

Author contributions

Yuhui Yi: theoretical calculation, methodology, writing (original draft preparation); Jie Wang: experimentation, writing (original draft preparation); Yingli Niu: theoretical calculation; Yu Yu: writing (review and editing); Songmei Wu: supervision, formal analysis, funding acquisition; Kejian Ding: supervision, conceptualization, project administration, writing (revision), Funding acquisition.

Conflicts of interest

There are no conflicts to declare.

Acknowledgements

The work described in this Letter was supported by Beijing Municipal Science and Technology Projects Commission (Z221100005222016), the National Key Research and Development Plan of China (2017YFC0805900), the National Natural Science Foundation of China (NSFC51972017, 21503013), and the Fundamental Research Funds for the Central Universities of China (2019JBM409, 2019JBM326).

References

1 L. Feng, Q. Yuanyuan and Z. Mingwen, *Carbon*, 2015, **95**, 51–57.
2 W. Yan, Y. Yu, H. Zou, X. Wang, P. Li, W. Gao, J. Wang, S. Wu and K. Ding, *Sol. RRL*, 2018, **2**, 1800058.
3 A. Fischer, M. Antonietti and A. Thomas, *Adv. Mater.*, 2007, **19**, 264–267.
4 D. M. Teter and R. J. Hemley, *Science*, 1996, **271**, 53–55.
5 I. Alves, G. Demazeau, B. Tanguy and F. Weill, *Solid State Commun.*, 1999, **109**, 697–701.
6 J. Ortega and O. F. Sankey, *Phys. Rev. B*, 1995, **51**, 2624–2627.
7 J. E. Lowther, *Phys. Rev. B*, 1999, **59**, 11683–11686.
8 E. Kroke, M. Schwarz, E. Horath-Bordon, P. Kroll, B. Noll and A. D. Norman, *New J. Chem.*, 2002, **26**, 508–512.
9 B. V. Lotsch, M. Döblinger, J. Sehnert, L. Seyfarth, J. Senker, O. Oeckler and W. Schnick, *Chem.–Eur. J.*, 2007, **13**, 4969–4980.
10 F. Fina, S. K. Callear, G. M. Carins and J. T. S. Irvine, *Chem. Mater.*, 2015, **27**, 2612–2618.
11 M. J. Bojdys, J.-O. Müller, M. Antonietti and A. Thomas, *Chem.–Eur. J.*, 2008, **14**, 8177–8182.
12 E. Wirnhier, M. Döblinger, D. Gunzelmann, J. Senker, B. V. Lotsch and W. Schnick, *Chem.–Eur. J.*, 2011, **17**, 3213–3221.
13 H. Schlomberg, J. Kröger, G. Savasci, M. W. Terban, S. Bette, I. Moudrakovski, V. Duppel, F. Podjaski, R. Siegel, J. Senker, R. E. Dinnebier, C. Ochsenfeld and B. V. Lotsch, *Chem. Mater.*, 2019, **31**, 7478–7486.
14 M. Döblinger, B. V. Lotsch, J. Wack, J. Thun, J. Senker and W. Schnick, *Chem. Commun.*, 2009, 1541–1543, DOI: 10.1039/B820032G.
15 B. Jürgens, E. Irran, J. Senker, P. Kroll, H. Müller and W. Schnick, *J. Am. Chem. Soc.*, 2003, **125**, 10288–10300.
16 M. Groenewolt and M. Antonietti, *Adv. Mater.*, 2005, **17**, 1789–1792.
17 T. Botari, W. P. Huhn, V. W.-h. Lau, B. V. Lotsch and V. Blum, *Chem. Mater.*, 2017, **29**, 4445–4453.
18 P. R. Tentscher and J. S. Arey, *J. Chem. Theory Comput.*, 2012, **8**, 2165–2179.
19 É. Brémond, M. Savarese, N. Q. Su, Á. J. Pérez-Jiménez, X. Xu, J. C. Sancho-García and C. Adamo, *J. Chem. Theory Comput.*, 2016, **12**, 459–465.
20 S. Vuckovic and K. Burke, *J. Phys. Chem. Lett.*, 2020, **11**, 9957–9964.
21 T. Lu and F. Chen, *J. Mol. Model.*, 2013, **19**, 5387–5395.
22 L. Simón and J. M. Goodman, *Org. Biomol. Chem.*, 2011, **9**, 689–700.
23 T. Lu and F. Chen, *J. Comput. Chem.*, 2012, **33**, 580–592.
24 A. P. Scott and L. Radom, *J. Phys. Chem.*, 1996, **100**, 16502–16513.
25 M. J. Frisch, G. W. Trucks, H. B. Schlegel, G. E. Scuseria, M. A. Robb, J. R. Cheeseman, G. Scalmani, V. Barone, G. A. Petersson, H. Nakatsuji, X. Li, M. Caricato, A. V. Marenich, J. Bloino, B. G. Janesko, R. Gomperts, B. Mennucci, H. P. Hratchian, J. V. Ortiz, A. F. Izmaylov, J. L. Sonnenberg, D. W. Young, F. Ding, F. Lipparini, F. Egidi, J. Goings, B. Peng, A. Petrone, T. Henderson, D. Ranasinghe, V. G. Zakrzewski, J. Gao, N. Rega, G. Zheng, W. Liang, M. Hada, M. Ehara, K. Toyota, R. Fukuda, J. Hasegawa, M. Ishida, T. Nakajima, Y. Honda, O. Kitao, H. Nakai, T. Vreven, K. Throssell, J. A. Montgomery Jr, J. E. Peralta, F. Ogliaro, M. J. Bearpark, J. J. Heyd, E. N. Brothers, K. N. Kudin, V. N. Staroverov, T. A. Keith, R. Kobayashi, J. Normand, K. Raghavachari, A. P. Rendell, J. C. Burant, S. S. Iyengar, J. Tomasi, M. Cossi, J. M. Millam, M. Klene, C. Adamo, R. Cammi, J. W. Ochterski, R. L. Martin, K. Morokuma, O. Farkas, J. B. Foresman and D. J. Fox, Gaussian, Inc., Wallingford CT, 2016.
26 G. Santra, N. Sylvetsky and J. M. L. Martin, *J. Phys. Chem. A*, 2019, **123**, 5129–5143.
27 T. Lu and Q. Chen, *Comput. Theor. Chem.*, 2021, **1200**, 113249.
28 C. Y. Legault, *CYLview20*, Université de Sherbrooke, 2020.
29 T. Lu, *Molclus program, Version 1.9.9.5*, 2022.
30 S. Grimme, C. Bannwarth and P. Shushkov, *J. Chem. Theory Comput.*, 2017, **13**, 1989–2009.
31 C. Bannwarth, S. Ehlert and S. Grimme, *J. Chem. Theory Comput.*, 2019, **15**, 1652–1671.
32 C. Bannwarth, E. Caldeweyher, S. Ehlert, A. Hansen, P. Pracht, J. Seibert, S. Spicher and S. Grimme, *Wiley Interdiscip. Rev.: Comput. Mol. Sci.*, 2021, **11**, e1493.
33 T. Lu and Q. Chen, *Chem. Methods*, 2021, **1**, 231–239.
34 W. Humphrey, A. Dalke and K. Schulten, *J. Mol. Graphics*, 1996, **14**, 33–38.

35 R. G. Van, F. L. Drake, *Python 3 Reference Manual*, CreateSpace, Scotts Valley, 2009, vol. 10, p. 1593511.
36 N. E. Henriksen and F. Y. Hansen, *Theories of molecular reaction dynamics: the microscopic foundation of chemical kinetics*, Oxford University Press, 2nd edn, 2018.
37 B. V. Lotsch and W. Schnick, *Chem.–Eur. J.*, 2007, **13**, 4956–4968.
38 E. Wirnhier, M. B. Mesch, J. Senker and W. Schnick, *Chem.–Eur. J.*, 2013, **19**, 2041–2049.
39 M. B. Smith, *March's advanced organic chemistry: reactions, mechanisms, and structure*, John Wiley & Sons, 8th edn, 2020.
40 H. Kruse, L. Goerigk and S. Grimme, *J. Org. Chem.*, 2012, **77**, 10824–10834.
41 G. Socrates, *Infrared and Raman characteristic group frequencies: tables and charts*, John Wiley & Sons, 2004.